UC San Diego

UC San Diego Electronic Theses and Dissertations

Title

Exploring the Reprogramming of hiPSCs to Hair Cell- and Spiral Ganglion-like Cells through Combinatorial Transcription Factor Overexpression

Permalink

https://escholarship.org/uc/item/44s4f6tp

Author

Kim, Grace

Publication Date

2024

Peer reviewed|Thesis/dissertation

eScholarship.org Powered by the California Digital Library
University of California

UNIVERSITY OF CALIFORNIA SAN DIEGO

Exploring the Reprogramming of hiPSCs to Hair Cell- and Spiral Ganglion-like Cells through Combinatorial Transcription Factor Overexpression

A thesis submitted in partial satisfaction of the requirements for the degree Master of Science

in

Biology

by

Grace Kim

Committee in charge:

Professor Karl Jonas Wahlin, Chair
Professor Randolph Hampton, Co-Chair
Professor Michael William Perry

2024

The thesis of Grace Kim is approved, and it is acceptable in quality and form for publication on microfilm and electronically.

University of California San Diego
2024

TABLE OF CONTENTS

THESIS APPROVAL PAGE iii
TABLE OF CONTENTS iv
LIST OF FIGURES v
ACKNOWLEDGEMENTS vi
ABSTRACT OF THE THESIS vii
Introduction 1
Materials & Methods 5
Cell Line 5
Reporter Line 5
Maintenance of hiPSCs 5
Generation of Tet-Inducible Transgene Donor Plasmids 6
Preparation of Transfection-Ready Plasmids 7
Stable Integration of Transgene Cassettes 7
Direct Conversion of hiPSCs to APG1 and NAN1 induced cells 7
Clonal Selection 8
Immunocytochemistry and Imaging 9
Bulk RNA-sequencing 9
Bulk RNA-sequencing analysis 10
Results 12
Overexpression of APG1 and NAN1 in hiPSCs leads to distinct morphologies during differentiation 12
APG1 induced cells exhibit auditory processes 13
APG1 and NAN1 induced cells express both neuronal and sensory markers 15
Transcriptomic profiles of APG1 and NAN1 overlap more at day 14 of differentiation 18
Discussion 22
Figures 25
References 33

LIST OF FIGURES

Figure 1: Overview of the inner ear structure and development in mammals.....25

Figure 2: Morphological changes of IMR90.4 *APG1* and *NAN1* cell lines upon differentiation....27

Figure 3: Comparative bulk RNA-seq analyses show *APG1* induced cells heading towards auditory cell fate.....29

Figure 4: *APG1* and *NAN1* express both HC- and SGN-related genes.....30

Figure 5: *APG1* and *NAN1* transcriptomic profiles at day 14 overlap with one another.....31

ACKNOWLEDGEMENTS

I would like to acknowledge Manan Chopra and Aleksandra Dragozova for their support and bioinformatics knowledge that helped me to write this thesis. I would like to acknowledge Devansh Agarwal for his continued mentorship throughout the years since I first joined the Wahlin lab. I would like to acknowledge Nathan Kemmerer for his help in growing, differentiating, and staining some of the *APG1* and *NAN1* induced cells. I would like to acknowledge Veda Palaparty and Avel Mandap on their help on cloning some of the plasmid constructs. I would like to acknowledge Dr. Randolph Hampton and Dr. Michael Perry for accepting to be on my committee and attending my defense. I would like to acknowledge my advisor, Dr. Karl Wahlin, for providing me with this research opportunity as well as his guidance over the years.

ABSTRACT OF THE THESIS

Exploring the Reprogramming of hiPSCs to Hair Cell- and Spiral Ganglion-like Cells through Combinatorial Transcription Factor Overexpression

by

Grace Kim

Master of Science in Biology

University of California San Diego, 2024

Professor Karl Jonas Wahlin, Chair
Professor Randolph Hampton, Co-Chair

The loss of hair cells (HCs) and spiral ganglion neurons (SGNs) in the inner ear can lead to irreversible hearing loss in mammals. Because these cells are few in number and difficult to access, studies on their development, degeneration, and reprogramming capabilities in response to injury have been limited. Previous studies have analyzed the gene expression profiles of HCs and SGNs in mice through bulk and single-cell RNA sequencing, with some identifying transcription factor (TF) genes, such as *Atoh1*, *Pou4f3*, *Gfi1*, *Neurog1*, and *Neurod1* as significant for HC and SGN development and maturation. However, it is not known whether these findings apply to the human system. Thus, a reliable and accurate *in vitro* model of human HCs and SGNs has yet to be generated to study their development and injury responses. In this study, we overexpressed two unique sets of TF gene cassettes in IMR90.4 cells with an

endogenous *POU4F3*-p2A-eGFP reporter: (1) TetO-*ATOH1*-p2A-*POU4F3*-p2A-*GFI1* (*APG1*) and (2) TetO-*NEUROG1*-p2A-*ATOH1*-p2A-*NEUROD1* (*NAN1*) for generation of HC- and SGN-like cells, respectively. These modified hiPSCs were differentiated and collected for bulk RNA-sequencing after 6 and 14 days. Sequencing analysis revealed that after six days, *APG1* induced cell gene expression was enriched for auditory processes, but this enrichment was less significant by day 14. Though day 6 *NAN1* induced cells appear more neuronal than day 6 *APG1* cells, possibly leading to an SGN-like cell fate, they do not take on a definitive cell type identity, instead expressing some HC- and neuronal genes at days 6 and 14.

Introduction

Hearing loss affects approximately 1.57 billion people worldwide and is postulated to almost double in prevalence by 2050[1]. Auditory deprivation has been associated with increased unemployment rates and risk of dementia as well as feelings of isolation, depression, and anxiety[2–8]. Though hearing loss has varying etiologies, including genetics and excessive noise, it can be tied to one principal cause: damage or loss of sensorineural cells in the inner ear[9].

The inner ear is composed of the cochlea and vestibule (**Fig. 1A**), which are responsible for processing sound and establishing balance, respectively. These functions are made possible through mechanosensory cells called hair cells (HCs). Within the cochlea, one row of inner hair cells (IHCs) and three rows of outer hair cells (OHCs) constitute the Organ of Corti. While IHCs are responsible for much of the mechanotransduction process, whereby sound waves are converted to electrochemical signals, OHCs are responsible for sound amplification and fine-tuning[10]. Adjacent to the HCs, supporting cells (SCs) maintain the homeostatic environment of the Organ of Corti and provide structural integrity, mechanical protection, and metabolic support to the HCs[11]. Both IHCs and OHCs innervate the spiral ganglion neurons (SGNs), which relay the electrochemical signals to the auditory cortex of the brain.

In mammals, the inner ear derives from a thickening of the surface ectoderm near the hindbrain. This thickening epithelium known as the otic placode invaginates to form the otic cup and later a vesicle called an otocyst. Anterior-posterior axial specification is one of the first events to occur during this process and is important for establishing the neural-sensory domain of the anterior region[12]. Cells within this domain initially express otic progenitor genes, such as *Lfng*, *Six1*, *Sox2*, and *Eya1*[13–15]. Later, some begin to express the proneural gene, *Neurog1*, that convert them into neuroblasts (**Fig. 1B**). These neuroblasts delaminate from the epithelium,

migrate out of the otocyst, and gather to form the cochleovestibular ganglion, from which cochlear neurons mature into either Type Ia, Ib, Ic or Type II SGNs[12,16–19]. The remaining cells in the neural-sensory domain begin expressing *Atoh1*, which marks the start of sensory differentiation[20,21]. Some of these "prosensory cells" express a cascade of TFs that separate them into either mature HCs or SCs. The mature HCs undergo further specification into IHCs or OHCs[22,23] (**Fig. 1B**).

In the mammalian inner ear, HCs and SGNs are post-mitotic and do not regenerate after injury or loss. On the contrary, lower vertebrate species, such as chicks and amphibians, have been shown to endogenously regenerate HCs and SGNs after injury. For example, past studies suggest that regeneration of HCs occurs through two mechanisms: (1) direct transdifferentiation of SCs to HCs and (2) re-entrance of SCs into the cell cycle and subsequent differentiation of their daughter cells to both HCs and SCs[24]. As such regenerative capacity is severely limited in adult mammals, much research has attempted to recapitulate endogenous regeneration of mammalian sensorineural cells, particularly in mice.

However, there is still limited knowledge on the development, reprogramming, and regenerative capabilities of the human inner ear system, partly due to the scarcity of HCs and difficulty in accessing the inner ear. Thus, this study aims to generate an *in vitro* model of human HCs and SGNs that could be used for various applications, including neuroprotective drug testing, creation of injury and developmental models, *in vivo* transplantation, and ultimately, regeneration.

One potential way to generate human HCs *in vitro* is to overexpress a select combination of transcription factors (TFs) in human induced pluripotent stem cells (hiPSCs) and forcefully convert them into mature HCs. Gene expression profiles in mouse HCs suggest that the TFs,

Atoh1, *Pou4f3*, and *Gfi1* play critical roles in HC development[25–29]. These studies have shown that *Atoh1* is responsible for committing otic progenitors to a sensory fate and activating the downstream TF, *Pou4f3*, which in turn activates *Gfi1* to generate mature HCs (**Fig. 1B**). It was found that *Gfi1* represses genes involved in neural development while upregulating HC-characteristic genes for their proper differentiation[30]. However, we do not know whether these findings apply to the development of human HCs. Thus, the human counterparts of the three TFs–*ATOH1*, *POU4F3*, and *GFI1*–have been selected in our study to determine whether this combination can convert hiPSCs into HC-like cells.

In addition, the proneural TF genes, *Neurog1* and *Neurod1*, have been implicated in SGN development in mice[31–33]. As hearing loss can be attributed to SGN damage, *NEUROG1* and *NEUROD1* have also been included in our study. Past studies on mice inner ear development suggest that *Neurog1* precedes *Atoh1* expression, and their roles in cell fate specification are mutually exclusive. While *Neurog1* pushes otic progenitors towards a neural fate, *Atoh1* directs them towards a sensory one. However, the spatial and cellular expression patterns of these two TFs might not be so straightforward, as a previous study by Raft et al. showed that HCs within the utricle and saccule of the vestibular system derive from otic progenitors that once expressed *Neurog1*[34]. Using a lineage trace reporter system in developing mice, they found that subsequent expression of *Atoh1* in "*Neurog1* derivatives" directs them to a sensory fate. This suggests that HCs and neurons within the vestibule develop from a common progenitor pool, and *Atoh1* is sufficient to push neural progenitors towards becoming HCs. Such findings have not been shown in the cochlea. In addition, though *Neurod1* is defined as a proneural gene, it also plays an important role in early HC development[35,36]. Given the complex interactions among these TFs,

much is yet to be discovered about the gene regulatory network of mammalian HC and SGN development.

Thus, two different combinations of TF genes were overexpressed in IMR90.4 cells with a *POU4F3*-p2A-eGFP reporter to generate HC- and SGN-like cells: (1) *ATOH1*-p2A-*POU4F3*-p2A-*GFI1* (*APG1*) and (2) *NEUROG1*-p2A-*ATOH1*-p2A-*NEUROD1* (*NAN1*), respectively, with both regulated by a tetracycline-inducible promoter. These hiPSCs were differentiated in the presence of small molecules blocking the BMP pathway, then collected for bulk RNA-sequencing (RNA-seq) at days 6 and 14. Comparison of their expression with that of undifferentiated hiPSCs, a control line differentiated as above but lacking any transgenes, and retinal ganglion cell-induced neurons (RGC-iNs)[37] showed that each possessed a different transcriptional profile. Further analysis revealed that after six days, *APG1* induced cell gene expression was enriched for auditory processes, but this enrichment was less significant by day 14. On the other hand, though day 6 *NAN1* induced cells appear more neuronal than day 6 *APG1* cells, possibly leading to an SGN-like cell fate, they do not take on a definitive cell type identity, instead expressing some HC- and neuronal genes at days 6 and 14.

Materials & Methods

Cell Line

IMR90.4 hiPSCs were used in this study and regularly checked for mycoplasma by PCR analysis.

Reporter Line

POU4F3-p2A-eGFP reporter cells in the IMR90.4 background were previously genotyped and sequenced in our lab, but their use has not been verified outside of this experiment.

Maintenance of hiPSCs

hiPSCs were maintained on 1% (vol/vol) Matrigel (MG)-GFR (#354230; Corning) extracellular matrix (ECM) coated plates in hypoxic condition (5% O_2 and 10% CO_2) at 37°C. They were fed daily with B8 media free of antibiotics[38]. For routine, clump passaging of stem cells (every 3-4 days), they were treated with a homemade cell-dissociation buffer for 6-7 minutes when the cells reached ~70% confluency. The cells were plated in (MG)-GFR coated wells containing B8 media with thiazovivin (LC Laboratories) (B8T), a ROCK inhibitor that promotes cell adhesion and survival[39]. For single-cell dissociation of stem cells, they were treated with Accutase (#A6964; Sigma) for 10-12 minutes, quenched with B8T, pelleted at 80xg for 5 minutes, and resuspended with B8T before plating 3000 cells/well in a 12-well plate or 7000 cells/well in a 6-well plate. The day after passaging, the B8T media was exchanged for B8 media.

Generation of Tet-Inducible Transgene Donor Plasmids

Transgene sequences, *NEUROG1*, *ATOH1*, and *POU4F3*, were PCR amplified from genomic DNA isolated from stem cells. The human *POU4F3* gene contains two coding exons. Subsequently, exon 1 was amplified separately from exon 2 and assembled into one continuous sequence using overlap extension PCR. *NEUROD1* was amplified from cDNA pooled from day 18-45 optic vesicles[40]. To generate the cDNA library, cells from optic vesicles were lysed, and their total RNA was isolated and reverse transcribed into cDNA, using the Quick-RNA Miniprep Kit (R1054; Zymo Research) and SuperScript IV reverse transcriptase (#18090050, Thermo Fisher Scientific), respectively. The *GFI1* gene was synthesized *de novo* via Twist Bioscience and PCR amplified using our selected cloning oligos. All PCR amplifications, including our plasmid backbones, were performed using Phusion Flash High-Fidelity PCR Master Mix (#F548L; Thermo Fisher Scientific) and purified with DNA Clean & Concentrator-5 (#D4013; Zymo Research). Inserts were ligated into desired backbones using a homemade Gibson assembly mix as previously described[37], after which the Gibson reaction mix was digested with DpnI enzyme (#R0176L; NEB) to remove any remaining methylated parental plasmids. Plasmids were transformed into NEB Stable Competent *E. coli* bacteria, miniprepped using ZymoPURE Plasmid Miniprep kit (#D4210; Zymo Research) and sequenced via Sanger sequencing (Eurofins Genomics) and whole plasmid next generation sequencing (Primordium Labs).

Both transgene donor plasmids used in this experiment were designed with polycistronic (p2A) sequences in between the genes: (1) *ATOH1*-p2A-*POU4F3*-p2A-*GFI1* (*APG1*) and (2) *NEUROG1*-p2A-*ATOH1*-p2A-*NEUROD1* (*NAN1*). Expression of each transgene cassette was regulated by a Tet-inducible promoter upstream of the genes. After PCR amplification of each

component, the DNA fragments were assembled via overlap extension PCR to generate two unique transgene cassettes.

Preparation of Transfection-Ready Plasmids

Sanger sequence-verified plasmids were clonally amplified in NEB Stable Competent *E. coli* bacteria grown at 37°C for 12-16 hours in LB. The cultures were spun down at 3200xg for 10 minutes at room temperature. ZymoPURE II Plasmid Midiprep kit (D4200; Zymo Research) was used to column purify the plasmids, which were also run through an endotoxin removal column at the end of the Midiprep. Before transfection, purified plasmids were sent for whole-plasmid, next generation sequencing to Primordium Labs.

Stable Integration of Transgene Cassettes

IMR90.4 *POU4F3*-p2A-eGFP cells with constitutively expressed rtTA-M2 at the AAVS1 locus[41] were transfected with 1 ug of pY026 EnAsCpf1(Cas12a) CLYBL-T1 catRNA plasmid, as previously modified[37], and 3 ug of CLYBL-TetO donor plasmid containing either *APG1* or *NAN1*. The CLYBL-TetO donor plasmid contains a constitutively expressed zeocin resistance marker. After electroporation of stem cells, they were treated with zeocin (200 μg/ml; InvivoGen) until cell death was no longer observed (~2 weeks). Acquisition of zeocin resistance indicated stable integration of the Tet-inducible transgene cassettes.

Direct Conversion of hiPSCs to *APG1* and *NAN1* induced cells

Zeocin-resistant cells were grown to 70-80% confluency and treated with LDN-193189 (100 nM; #SML0559; Sigma) and doxycycline (dox; 1μg/ml; #D5207; Sigma) in B6 media (B8 without growth factors). After 16-24 hours, pre-treated cells were single-cell passaged with Accutase for 12 minutes, pelleted at 80-100xg for 5 minutes, and quenched with neural induction

medium (NIM)[37] containing dox and thiazovivin. Cells were passed once through a 35 μm cell strainer (#352235; Falcon). A hemocytometer was used to count the total number of cells. About 21,000 cells were plated into a single well of a 12-well plate that was coated with poly-L-ornithine (0.2 mg/ml; #P3655; Sigma) overnight, washed 3x with sterile cell-culture grade water, and coated with 1% (MG)-GFR. Cells were plated into induction medium, which contains NIM, dox, thiazovivin, 1x CultureOne supplement (#A3320201; Gibco), and LDN-193189. Two days after plating (Day 2), an additional 1 mL of induction medium was added to each well. A one-third media exchange was performed every other day after that with induction medium until day 6, at which point, the media exchange was performed with BrainPhys (#05790; StemCell Technologies) containing 10 nM nicotinamide (#72340; Sigma), B27 supplement[42,43], BDNF (50 ng/ml; #Qk050; Qkine), GDNF (10 ng/ml; #Qk051; Qkine), and dox. All cultures were kept in 5% O_2/10% CO_2 hypoxic conditions at 37°C.

Clonal Selection

To isolate a population of hiPSCs that show robust neural and neuroepithelial-like conversion, individual colonies of zeocin-resistant cells were selected and differentiated. For clonal selection, cells were single-cell passaged with Accutase and plated onto a 6-well plate with ~7000 cells per well. Once colonies had grown enough without touching the neighboring colonies, they were lifted off the well with a cell scraper (#89260; VWR). With a P1000 wide bore pipette tip, the lifted colonies were transferred to a 35-mm polystyrene petri dish. In a sterile laminar flow hood, colonies were viewed under a brightfield inverted microscope at 4x magnification and picked one-by-one with a P20 pipette tip. Each colony was transferred to a well in a 24-well plate (1 colony per well). Once the colonies reached ~70% confluency, they were clump-passaged onto two 24-well plates–one for maintenance and the other for

differentiation. Upon differentiation, colonies with the most robust neural and neuroepithelial-like conversion were selected for expansion and future experiments.

Immunocytochemistry and Imaging

Cells were fixed in 4% paraformaldehyde (PFA) in 0.1M Sorenson's buffer and 5% sucrose for 15-20 minutes. They were rinsed 3 times with 5% sucrose in Sorenson's buffer then incubated for 30 minutes at room temperature with a blocking solution containing 0.1% TritonX-100 (Sigma Aldrich #T8787) diluted in 1x DPBS and 2% normal horse serum (NHS). After cells were rinsed once with 1x DPBS, they were stored overnight at 4°C in 0.1% TritonX-100 with 2% NHS and 1:50 mouse monoclonal anti-*MYO7A* (DSHB; #MYO7A 138-1-s) and 1:1000 mouse monoclonal anti-TUJ1 (Covance; #MMS-435P). The secondary antibody, anti-mouse IgG coupled to Alexa Fluor 647 (Invitrogen, 1:2000), was combined with 10 ug/ml of 4',6-diamidino-2-phenylindole (DAPI; Roche) diluted in 1x DPBS. After removal of the primary antibody solution, cells were rinsed once with DPBS and incubated in the secondary antibody solution for 1 hour at room temperature away from light. Cells were rinsed again with DPBS and left in 5% sucrose in Sorenson's buffer at 4°C until ready to be imaged. ImageXpress Micro Confocal High-Content Imaging System (Molecular Devices) was used to acquire images of the cells. Images were adjusted for brightness and contrast and pseudocolored using ImageJ and Affinity Designer. Brightfield images of hiPSCs and differentiated cells were acquired with a Leica DMi1 inverted microscope.

Bulk RNA-sequencing

Differentiated controls (CTL) at days 6 (n=3) and 14 (n=3), *APG1* induced cells at days 6 (n=3) and 14 (n=3) as well as *NAN1* induced cells at days 6 (n=3) and 14 (n=3) were collected

for bulk RNA-seq. The Quick RNA Microprep Kit (Zymo Research; #R1050) was used per the manufacturer's instructions to extract RNA from each sample. RNA quantity and quality were evaluated using NanoDrop 2000 (Thermo Scientific) and 4200 TapeStation (Agilent Technologies), respectively. Sequencing libraries were generated using the NEBNext Ultra II Directional RNA Library Prep Kit (#E7760L; NEB). Sequencing was performed on a NovaSeq X Plus (100 bp paired-end reads, Illumina) at the UCSD Institute for Genomic Medicine (IGM) Core to obtain ~35 million reads per sample.

Bulk RNA-sequencing analysis

Raw sequencing reads were downloaded as FASTQ files, and adapters were trimmed using TrimGalore! (Galaxy Version 0.6.3). Sequencing reads were then aligned to the human reference genome GRCh38.p13 via HISAT2 (Galaxy Version 2.2.1). FeatureCounts (Galaxy Version 2.0.1+) was used to quantify the expression counts for each gene. Differential gene expression (DGE) analysis between the collected treatment groups (CTL, *APG1*, *NAN1*) was performed through DESeq2 (Galaxy Version 2.11.40.6). Untreated PSCs and *NAIP2* induced neurons (RGC-iNs) at day 6 (n=4) and day 14 (n=4) from a previous study were also included in the DGE analysis. Principal Component Analysis (PCA) plots were generated using DESeq2. Hierarchical cluster analysis was performed using Seaborn (Version 0.12.0) and Matplotlib (Version 3.6.0) in Python, which was then used to generate heatmaps of differentially expressed genes (DEGs). Venn diagrams were created from VennPainer (Version 1.2.0). Normalized counts of genes for each treatment group across replicates were inputted into GraphPad Prism 10 (Version 10.2.3) to generate bar charts and line graphs. DESeq2 was also used to obtain differential expression data including $\log_2$(fold change, FC), false discovery rate, and adjusted p-values. Significant DEGs with normalized counts >10, a $\log_2$(FC) >1, and an FDR <0.05 were

inputted into GSEApy (Version 1.0.4) to identify biological pathways significantly overrepresented in *APG1* and *NAN1* groups as defined by Gene Ontology. Bar charts of the top 10 significantly differentially expressed pathways (FDR <0.05) were created through Seaborn and Matplotlib.

Results

Overexpression of *APG1* and *NAN1* in hiPSCs leads to distinct morphologies during differentiation

To further explore the combinatorial effects of inner ear-related TFs in the human system, we designed two transgene cassettes for integration and overexpression in IMR90.4 *POU4F3*-p2A-eGFP cells. The 'hair-cell' cassette contains *ATOH1*, *POU4F3*, and *GFI1* (*APG1*) (**Fig. 2A**), three TF genes known to participate in HC development and maturation. The second cassette contains *NEUROG1*, *ATOH1*, and *NEUROD1* (*NAN1*) (**Fig. 2A**), which we postulated will lead to SGN-like cells. Within each cassette, genes were linked together via polycistronic (p2A) sequences, which allowed them to be transcribed as a single mRNA transcript and translated as separate proteins simultaneously. The transgene cassettes were each coupled with a dox-inducible third-generation Tet-ON (TetO) promoter (**Fig. 2A**). Using a high-fidelity EnCas12a gene knock-in system, *APG1* and *NAN1* were integrated into the Citramalyl-CoA Lyase (CLYBL) safe harbor site in IMR90.4 *POU4F3*-p2A-eGFP reporter cells (**Fig. 2A**). The CLYBL site has been verified for use in hiPSCs, and integration of transgenes into this site allows for inducible transgene expression without disrupt of other endogenous genes[44]. The two cell lines were validated for stable integration of *APG1* and *NAN1* via zeocin resistance and PCR analysis.

A previous study in our lab showed that synchronous BMP inhibition and overexpression of four TFs (*NEUROG2*, *ATOH7*, *ISL1*, and *POU4F2* or *NAIP2)* can lead to efficient conversion of hiPSCs into induced neurons (iNs) and retinal ganglion cells (RGC-iNs). Thus, in our attempt to generate SGNs, we treated IMR90.4 *NAN1* cells with LDN and dox (**Fig. 2B**). Over time, neuronal features were observed in *NAN1* cells, including neurite outgrowth from their cell

bodies. By day 4, neurites grew extensively longer compared to those at days 1 and 3 (**Fig. 2C**). This indicated that iNs can be generated from stem cells by overexpressing the TF gene cassette, *NEUROG1*-p2A-*ATOH1*-p2A-*NEUROD1*. Previous studies have also shown that BMP inhibition is also important for HC differentiation[45], thus IMR90.4 *APG1* cells were also treated with LDN and dox. In contrast to *NAN1, APG1* cells do not show distinct somas and long bipolar neurite outgrowth. Their cell bodies are flatter and congregate together, and the spindly outgrowths were observed to fasciculate together at day 5 (**Fig. 2C**). However, by day 14, it appeared that *APG1* cells acquired a neuronal morphology similar to *NAN1*, though the cell bodies were much more bundled together in *APG1* cells.

APG1 induced cells exhibit auditory processes

Bulk RNA-seq was carried out on *APG1* and *NAN1* induced cells to elucidate their transcriptional profiles. Within the RNA-seq analyses, day 6 *APG1* samples (n=3) were compared with day 6 *NAN1* (n=3) and a previously collected day 6 *NAIP2* dataset (n=4). PSCs (n=3) and dox-treated CTL (n=3) samples were also included. Principal component analysis (PCA) of the 5 treatment groups shows a total of 78% variance, with induced cells clustering separately from the CTLs and PSCs (**Fig. 3A**). The variance amongst the *APG1*, *NAN1*, and *NAIP2* expressing cells increases to a total of 96% when CTLs and PSCs are removed, and three distinctly separated clusters are apparent. Replicates within each sample cluster together, indicating low variance (**Fig. 3A**). While all 5 treatment groups share a considerable number of genes, they each express a unique set of genes as well, as shown in the Venn Diagram (**Fig. 3B**; normalized count > 100). A global heatmap of the top 500 DEGs in *APG1* induced cells shows that day 6 *APG1*, *NAN1*, and *NAIP2* groups are clustered separately from PSC and CTL groups (**Fig. 3C**).

Next, to further explore the identities of *APG1* and *NAN1* induced cells, Gene Set Enrichment Analysis (GSEA) was performed. Ranked lists of DEGs in the day 6 *NAN1* group vs. *NAIP2* and *APG1* were inputted into GSEApy to obtain the top significant biological pathways upregulated in *NAN1*, as defined by Gene Ontology. A similar method was used to generate significantly upregulated pathways in *APG1*. Only four biological pathways were significantly upregulated in *NAN1* compared to *NAIP2* and *APG1* groups, each (**Fig. 3D**). Most of these pathways, including cholesterol, secondary alcohol, and sterol biosynthetic processes (GO: 0006695, GO: 1902653, GO: 0016126), were too broad to decipher the possible cell fates *NAN1* induced cells were committing to. This may be because overexpression of *NEUROG1* and *ATOH1* in *NAN1* render them similar to *NAIP2* and *APG1* groups at this early stage of differentiation. To confirm that *NAN1* induced cells are heading towards neuronal development as predicted, the significantly overrepresented pathways in *NAN1* compared to the CTL were also generated from GSEApy, which showed mainly synaptic developmental processes, including chemical synaptic transmission (GO: 0007268), neurotransmitter secretion (GO: 0007269), signal release from synapse (GO: 0099643), among others. *APG1* comparisons to *NAIP2* and *NAN1* showed an enrichment of muscle-related pathways, including myofibril assembly (GO: 0030239), sarcomere organization (GO: 0045214), skeletal muscle tissue development (GO: 0007519), and muscle contraction (GO: 0006936) (**Fig. 3E**). Epithelial cell development was also significantly upregulated in *APG1* cells relative to *NAN1*, which corroborated with *APG1*'s epithelial-like morphology at day 5, as mentioned previously (**Fig. 2C**). Notably, the pathways involved in sensory perception of sound (GO: 0007605) and mechanical stimulus (GO: 0050954) were both within the top 10 significantly upregulated pathways in *APG1* induced cells when compared to *NAIP2* and *NAN1* (**Fig. 3E**). Enrichment

plots for the two pathways were generated for better visualization (**Fig. 3F**). Interestingly, *APG1* and *NAN1* comparisons to *NAIP2* show significant enrichment of genes in the calcium-independent cell-cell adhesion via plasma membrane pathway (GO: 0016338) (**Fig. 3D and E**). In both groups, the leading genes within this pathway belong to the claudin gene family, which encodes membrane proteins important for tight junction formation. Claudin proteins are primarily enriched in epithelial and endothelial cells to establish a selectively permeable barrier between intra- and extracellular environments. Previous studies have shown loss or mutation of claudin genes, such as *CLDN14* and *CLDN1*, is associated with hearing loss in vertebrates[46–48], but further research is needed to determine their expression patterns in HC development.

Next, a heat map was generated to visualize *APG1*'s leading genes within the sensory perception of sound and mechanical stimulus pathways (**Fig. 3G**). Gene expression counts normalized across rows were used to compare the expression levels between PSCs, CTL, *NAIP2*, *APG1*, and *NAN1* at day 6. This shows that not all genes within the two pathways have large or similar normalized counts within the *APG1* group. Rather, the differential expression between *APG1* and all other groups for the listed genes has pushed *APG1* towards exhibiting auditory processes relative to the other cell types. Overall, global and pathway analyses of *APG1* and *NAN1* induced cells have shown that these cell lines are different from one another and from PSCs, CTL, and *NAIP2* cells, with *APG1* induced cells heading towards a more auditory fate compared to *NAN1* at day 6 of differentiation.

APG1 and *NAN1* induced cells express both neuronal and sensory markers

Next, we looked at specific gene markers to validate whether the transcriptional profiles of *APG1* and *NAN1* reflect those of mammalian HCs and SGNs. Myosin-VIIA (*MYO7A*) is a frequently used HC marker, as the gene is expressed in both vestibular and cochlear HCs starting

early in the sensory development of the inner ear. *APG1* and *NAN1* induced cells were stained for DAPI and *MYO7A* at day 6 of their differentiation, and interestingly, both lines were *MYO7A*+ (**Fig. 4A**). Though we predicted *NAN1* induced cells to resemble SGN-like cells and thus be *MYO7A*-, the immunocytochemistry result is not surprising, as *Atoh1*+ cells in the mice inner ear have been shown to be positive for *Myo7a* as well[49]. Thus, the overexpression of *ATOH1* within *NAN1* and *APG1* cells may have led them both to be enriched with *MYO7A.* In addition, based on the gene expression counts normalized across rows, *NAN1* induced cells had on average, a significantly higher expression of *MYO7A* than *APG1* (**Fig. 4B**). Perhaps the slight variance among *APG1* replicates has contributed to the group's lower expression count compared to *NAN1*.

Since a single gene marker does not comprehensively identify a cell type, we looked at other HC-associated markers, comparing each treatment group's average expression levels (**Fig. 4B**). In contrast to the *APG1* group, *NAN1* did not express much of *LHX3* and *MYO15A*, nor did the other three treatment groups. We also looked at early HC markers—*SOX2*, *SIX1*, and *LMO1*—to get a sense of the maturity of day 6 *APG1* and *NAN1* induced cells. Across all three genes, *NAN1* had higher average expression counts than *APG1* (**Fig. 4B**). A heatmap was also included, showing the relative expression levels of the five treatment groups for TFs shown to be upregulated during embryonic and postnatal development in mouse HCs[27,49] (**Fig. 4C**). *APG1* and *NAN1* induced cells had comparable normalized expression levels for certain TF genes, such as *CTBP2*, *CASZ1*, and *TUB*, but for others, such as *BARHL1*, *LHX3*, *DDIT3*, and *POU4F2*, the *APG1* group had higher expression levels. This shows that combinatorial overexpression of select TF genes within hiPSCs can lead to activation of a network of other TF genes to push cells into a desired cell fate.

NAN1 and *APG1* induced cells at day 6 were also stained for DAPI and a neuronal marker, *TUBB3* (**Fig. 4D**). In this case as well, both lines were *TUBB3*+, which was not surprising as *NAN1* was expected to be neuronal and *APG1* cells may still be at an early stage of their differentiation. Nascent HCs in chicks have been shown to be positive for TUBB3 and MYO7A simultaneously[50]. The five treatment groups' average gene expression counts for pan-neuronal markers were also included for more comprehensive profiling of the cells (**Fig. 4E**). Though *NAN1* had higher average expression levels for *TUBB3*, *MAP2*, *NCAM1*, *SYN1*, and *SYT1* than *APG1* cells, the *APG1* group also showed considerable expression of these neuronal markers with *APG1* having the highest normalized counts for *RBFOX3*. Perhaps this is due to the complex targetome of the ATOH1 TF, which not only activates genes involved in inner ear sensory development but also neuronal development[51]. In addition, since HCs share many neuronal functions, such as signal transduction, synapse formation, and synaptic vesicle trafficking, and are innervated by afferent nerve fibers, *APG1*'s expression of neuronal genes may not be unexpected.

Following these results, we looked at the average expression levels of *APG1* and *NAN1* induced cells for other HC- and SGN-associated genes to assess the stage of their differentiation and determine whether they are heading towards their predicted cell fates. The heatmap shows a list of genes that were constantly expressed in mice SGNs throughout their development[52] (**Fig. 4F**). Many neuronal genes, such as *ELAVL4*, *LRRC55*, *NRG1*, *SOGA3*, and *LINGO1* are shared between *NAN1* and *NAIP2* induced cells, both expressing significant levels of each gene. *APG1* cells also share several genes with *NAN1* and *NAIP2* cells with moderate expression. However, it is not fully convincing that *NAN1* is heading towards an SGN fate since the other treatment groups have overlapping gene expression patterns. In addition, *NAN1* is not expressing a number

of other SGN markers, such as *SCRT1*, *LYPD1*, and *CALB1*. Rather, it appears that the transcriptomic profile of *NAN1* induced cells at day 6 does not favor that of either HCs or SGNs but resembles a "hybrid" of the two.

Transcriptomic profiles of *APG1* and *NAN1* overlap more at day 14 of differentiation

In TF-mediated reprogramming of hiPSCs, the gene expression profiles of differentiating cells can drastically change as the initially overexpressed TFs activate downstream secondary TFs and effector genes over time. To determine whether our *APG1* and *NAN1* induced cells are capable of maturing into HC- and/or SGN-like cells, we continued to treat the cells with dox past day 6 and collected them at day 14 for bulk RNA-seq analysis. The PCA plot shows that within the *NAIP2* and CTL groups, days 6 and 14 replicates appear to cluster separately from each other (**Fig. 5A**). However, such distinct separation of clusters is less apparent within the *APG1* and *NAN1* groups. Interestingly, it seems that *APG1* induced cells at day 14 are clustering closer to the *NAN1* groups. A heatmap of the top 500 DEGs in *APG1* also shows an increase in expression of overlapping genes between day 14 *APG1* and *NAN1* induced cells compared to their day 6 counterparts (**Fig. 5B**). To see if this change in global expression levels coincided with changes in expression of our selected TFs, we plotted the normalized counts of *ATOH1*, *POU4F3*, and *GFI1* in our *APG1* groups at days 6 and 14 and did the same for *NAN1* (**Fig. 5C**). Interestingly, even with continuous dox treatment, expression levels decreased for all our selected TFs from day 6 to 14. This pattern was also shared by *NAIP2* induced neurons in a past study[37], though their dox treatment was discontinued after day 6. The decrease in TF expression, regardless of continued dox treatment, may have occurred due to epigenetic silencing of the Tet promoter as have been reported before[53–55]. Whether expression of *APG1* or *NAN1* will later increase through an endogenous mechanism is uncertain.

GSEA was also carried out to explore changes in enriched biological pathways at day 14 (**Fig. 5D**). Both *APG1* and *NAN1* induced cells at day 14 were significantly enriched with genes involved in synaptic development compared to their day 6 counterparts. Though the sensory perception of mechanical stimulus pathway continues to be significantly upregulated in *APG1* induced cells at day 14, the sensory perception of sound pathway is no longer significantly overrepresented in *APG1* cells when compared to day 14 *NAN1* cells (**Fig. 5D**). However, actin filament-based transport (GO: 0099515) is newly included within the top 10 significantly enriched pathways in day 14 *APG1* cells, in which genes within the myosin superfamily predominate (**Fig. 5D**). Day 14 *NAN1* cells are significantly upregulated with genes involved in neuron development and synaptic transmission compared to day 14 *APG1* cells. However, other pathways, including cardiac muscle cell action potential, renal water homeostasis, and migration involved in sprouting angiogenesis, are also present within day 14 *NAN1* cells (**Fig. 5D**). This does not necessarily indicate that *NAN1* cells are committing towards a cardiac muscle or kidney cell fate, as genes within the pathways may serve multiple functions outside of the two organ systems. However, to ensure that our induced cells are not committing towards non-inner ear related cell fates, we looked at gene markers for the heart and kidney (**Fig. 5E**). As expected, *APG1* and *NAN1* induced cells have negligible normalized expression counts for the gene markers.

We also conducted a temporal analysis of the bulk RNA-seq data to track changes in expression for pan-neuronal and SGN-related genes between days 6 and 14 in *APG1* and *NAN1* cells (**Fig. 5E**). Both induced cells continue to highly express the pan-neuronal genes, *TUBB3*, *MAP2*, and *NCAM1*, at day 14 (**Fig. 5E**). In fact, there is no significant change to the genes' expression in *APG1* and *NAN1* groups over time, as shown by the $\log_2$(FC) values between the

two timepoints (**Fig. 5F**). *SYN1*, which has been noted to be involved in synaptic vesicle trafficking and present at the synapse between SGNs and HCs[56], is significantly upregulated in *APG1* and *NAN1* cells at day 14 (**Fig. 5E** and **5F**). While the neuronal marker, *RBFOX3*, is significantly downregulated in *APG1* induced cells at day 14 compared to day 6, it is more upregulated at day 14 in *NAN1* cells (**Fig. 5F**). This indicated that at day 14, the *APG1* and *NAN1* induced cells have not yet lost their early neuronal characteristics. Subsequently, we looked at the $\log_2$(FC) values for additional neural genes (**Fig. 5F**). These genes—*GAP43*, *NCAM1*, *ST18*, *INSM1*, *GFY*, and *LHX2*—have been shown to be upregulated in HCs of *Gfi1* knockout mice, suggesting that without *Gfi1*, HCs remain in their nascent state and continue to express neuronal genes[30]. Since our *APG1* induced cells should be overexpressing *GFI1*, we wanted to see if they would exhibit the opposite trend. For 4 out of 6 genes—*ST18*, *INSM1*, *GFY*, and *LHX2*—there was a significant downregulation in *APG1* cells from day 6 to day 14. However, for the *NAN1* group, only 2 out of 6 genes showed a significant downregulation. This suggested that *APG1* induced cells may be starting to lose their neuronal characteristics at day 14 due to the overexpression of *GFI1*. In addition, there is a possibility that day 14 *APG1* has reached a more mature point than *NAN1* along their differentiation path towards a HC-like fate. We also looked at some genes that were shown to be constantly and dynamically expressed in SGNs throughout mice inner ear development[52] (**Fig. 5E**). While the genes, *STMN4*, *MAFB*, and *DCX*, were highly expressed in early SGNs in mice, *CELF4*, *LYPD1*, and *NRN1* were expressed later in mature SGNs. *SCRT2*, *ELAVL4*, and *TAGLN3* were noted to be constantly expressed in developing mice SGNs. From day 6 to day 14, *APG1* and *NAN1* cells continue to express "SGN-constant" genes at varying degrees (**Fig. 5E**). There is a slight increase in expression for "SGN-later" genes, such as *CELF4* and *LYPD1*, but both *APG1* and *NAN1* continue to highly express

some “SGN-early” genes (**Fig. 5E**). Since both induced cell lines seem to follow a similar expression pattern, it cannot be concluded that one or the other is committing more towards an SGN fate.

Lastly, we wanted to explore whether *APG1* and *NAN1* cells at day 14 would begin to adopt a mature HC transcriptomic profile. The list of HC gene markers in the heat map has been verified in multiple studies, and the genes marked in red pertain to mechanoelectrical transduction (MET) channels at the tip links of HC stereocilia[57] (**Fig. 5F**). First, we observed that the expression of *ATOH1*, *POU4F3*, and *GFI1* decreases in *APG1* cells from day 6 to 14, even with continuous dox treatment. Downregulation of *ATOH1* is also observed in maturing cochlear HCs in mammals[58]. In addition, decreased expression of *POU4F3*, *EPS8L2*, *BARHL1*, *GFI1*, *MFNG*, and *MREG* in *APG1* cells reflect the pattern observed in bulk RNA-seq data of mice embryonic and postnatal HCs from a previous study by Scheffer et al., 2015[27]. Though a slight downregulation of *ATOH1* is observed in *NAN1* day 14 cells, the gene is still highly expressed, and it appears that its downstream TF genes, *POU4F3* and *GFI1*, have not been activated based on their low expression counts. However, day 14 *NAN1* expression patterns for other HC-related genes, including *CASZ1*, *MGAT5B*, *CACNB2*, and *JAG2*, follow that of day 14 *APG1* cells. Though GSEA results showed an enrichment of synaptic development pathways in both *APG1* and *NAN1* cells at day 14, it appears that genes related to synaptic vesicle transport, such as *SLC17A8*, as well as mechanotransduction channels, including *TMC1*, *TMIE*, *PCDH15*, and *LHFPL5*, still have minimal and/or unchanged expression levels in *APG1* and *NAN1* groups. Overall, *APG1* induced cells appear to follow some trends noted in mammalian HC development though are not fully mature at day 14. The expression profile of *NAN1* day 14 cells has a greater resemblance to that of *APG1* day 14 cells than it did for day 6.

Discussion

Overexpression of *APG1* and *NAN1* in hiPSCs and subsequent differentiation with small molecules, LDN and dox, resulted in neuroepithelial- and neural-like cells, respectively, with unique transcriptomic profiles at day 6 of their differentiation. Comparative analyses of their bulk RNA-seq data showed that *APG1* induced cells were enriched for genes involved in sensory perception of sound and mechanical stimulus pathways. Further analyses showed that neuronal and sensory-related genes were not restricted to *NAN1* and *APG1* cells, respectively. Rather, both induced cells at day 6 expressed a considerable number of neuronal, HC- and SGN-associated genes, including *TUBB3* and *MYO7A*. However, *NAN1* average expression counts for early prosensory markers were higher than *APG1*, suggesting that *NAN1* may be at a more immature differentiation state than *APG1*.

By day 14, the morphologies of both *APG1* and *NAN1* induced cells appeared neuronal with elongated and fasciculated neurites, though the cell bodies of *APG1* cells were more clustered together. The highly polarized morphology of HCs—epithelial cell body with stereociliary projections—was not at all apparent in *APG1* cells. A PCA plot including all treatment groups showed that *APG1* replicates at day 14 cluster closer to the *NAN1* group than those at day 6. Corroborating the structural development of their neurites, *APG1* and *NAN1* were significantly enriched with genes involved in synaptic development at day 14 compared to day 6. The sensory perception of sound pathway was no longer significantly overrepresented in *APG1* cells at day 14 when compared to *NAN1*, though the mechanical stimulus pathway was still present. The expression patterns of *APG1* and *NAN1* cells at day 14 resemble each other when looking at HC-related markers. Together, this data suggests that *APG1* overexpression together with BMP inhibition may not be sufficient to drive HC formation and maintenance.

Many studies on mice have shown that *Atoh1* is necessary and sufficient to reprogram embryonic stem cells, fibroblasts, or supporting cells to HC-like cells. However, others have also suggested that additional TF genes as well as the spatiotemporal patterning of *Atoh1* are important to generate mature, functional HC-like cells. Perhaps, the presence of *ATOH1* in *NAN1* cells has pushed them towards a sensory fate, rendering their transcriptomic profile to be similar to *APG1*'s profile. However, since *APG1* contains additional TF genes downstream of *ATOH1* (*POU4F3* and *GFI1*), they can differentiate more specifically towards the HC fate, hence the significant overrepresentation of sound and mechanical stimulus pathways in *APG1* early in their differentiation.

Regardless though, there are a few discrepancies within *APG1* differentiation that are concerning. Notably, their morphologies are more neuronal than epithelial as the induced cells mature, and at day 14, *APG1* cells are not upregulated in maturing HC genes. Perhaps, the cells need to be differentiated up to days 21 and 28 and collected for bulk RNA-seq, as our lab has previously shown that RGC-iNs are not mature until day 28[37]. The induction method can also be altered to mimic the development of HCs. In our experiment, LDN was used to block BMP signaling at the onset of hiPSC differentiation. Usually, LDN is used to promote neural differentiation from PSCs. Previous studies have shown that BMP4 is expressed in prosensory patches of the otic vesicle, and a balance between endogenous BMP4 expression and an exogenous BMP inhibitor, Noggin, is important to establish the correct number of sensory cells, including HCs[45]. Given that BMP suppression leads to reduced cell proliferation, cell-cycle withdrawal, and HC specification *in vivo*, addition of LDN may not hinder *APG1* differentiation to HC-like cells. Considering this, perhaps addition of other small molecules may be useful to further aid their specification. Other reprogramming studies have used retinoic acid (RA) or a

gamma-secretase inhibitor, such as LY411575, since RA and inhibition of Notch signaling have been shown to promote HC generation from SCs[59–61]. Other TF genes can also be added to the *APG1* combination, such as *BARHL1* and *LHX3*, to promote HC differentiation[62,63]. Alterations to the *NAN1* construct can also be made to generate SGN-like cells. Removal of *ATOH1* and addition of SGN-related genes, such as *DELTA1* or *POU4F1*, could push the cells towards a more neuronal fate without expression of HC genes, e.g., *MYO7A*.

Accurate *in vitro* generation of human HC- and SGN-like cells can have a myriad of implications, including drug testing, developmental and injury models, and regeneration. Currently, our lab is working to create brain-retina models as well as neural connections between RGC-iNs and thalamus in culture. Establishing connections between induced SGNs and HCs as well as RGCs and photoreceptors *in vitro* can help to model degenerative and congenital diseases, such as Usher's syndrome, which leads to both vision and hearing loss. In addition, once the necessary and sufficient TF genes are identified to generate functional HC- and SGN-like cells from hiPSCs, they can be tested *in vivo* through adeno-associated viruses (AAVs). Since AAVs can deliver genes to target cells without host genomic integration, they can be used for future regenerative studies, mainly to reprogram existing cells in the inner ear (i.e., supporting cells) to functional HC- and SGN-like cells.

Figures

Figure 1: Overview of the inner ear structure and development in mammals. (A) The anterior region (beige) of the otocyst gives rise to the inner ear structure, which contains five sensory organs. The Organ of Corti is located in the cochlea and consists of inner hair cells (IHCs), outer hair cells (OHCs), pillar cells (PCs), Deiters' cells (DCs), greater epithelial ridge cells (GERs), and dendrites of Type I and II spiral ganglion neurons (SGNs). The utricle and saccule each contain a macula that consists of vestibular HCs innervated by vestibular ganglion neurons (VGNs). Movement of the otolith structure allows for detection of linear acceleration. (B) Regionalized expression of select TFs (*Lfng*, *Sox2*, *Six1*, *Eya1*) defines the anterior domain of the otic placode. This domain gives rise to neural, sensory, and supporting cells through the regulation of various TFs and signaling pathways (not shown). Created with BioRender.com.

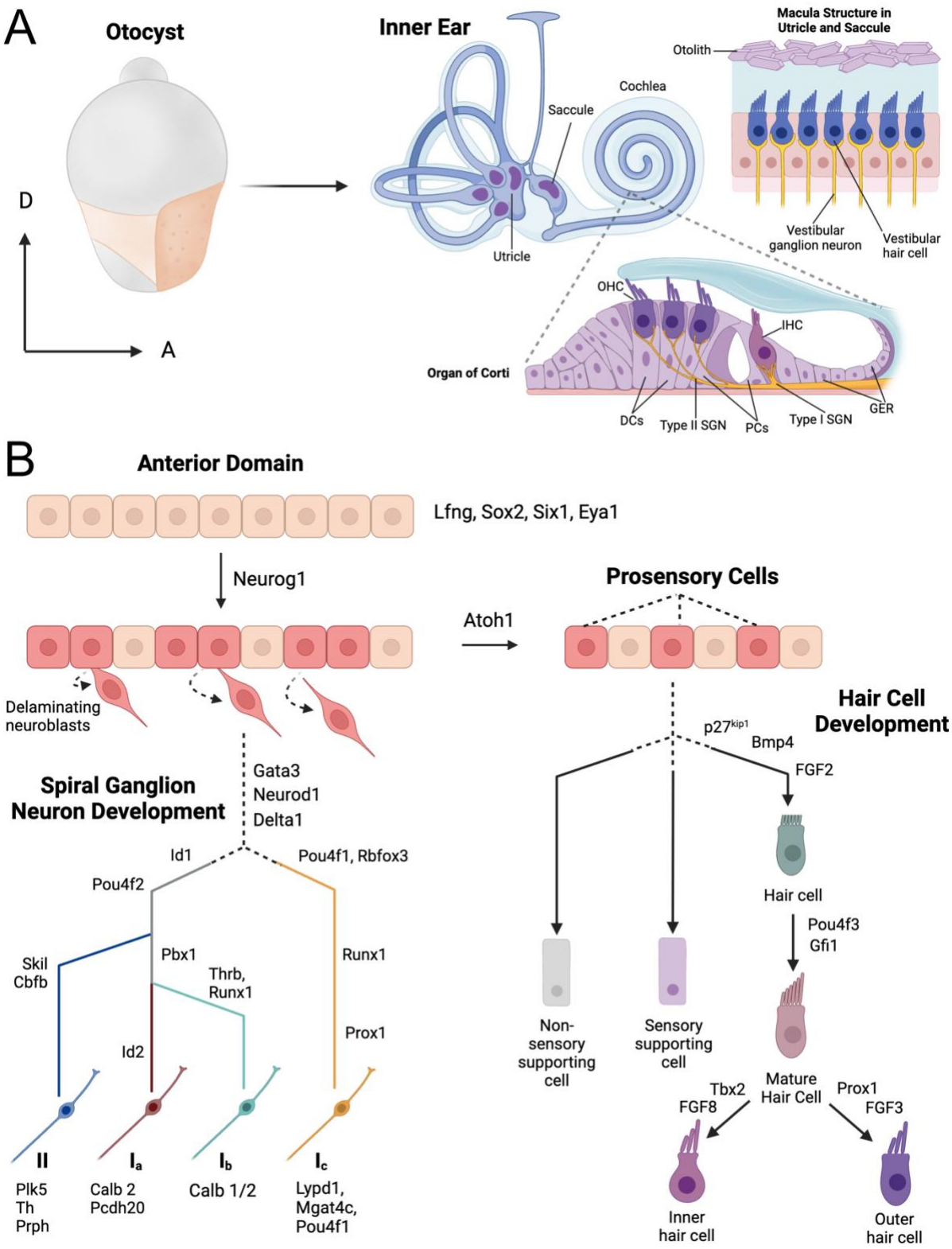
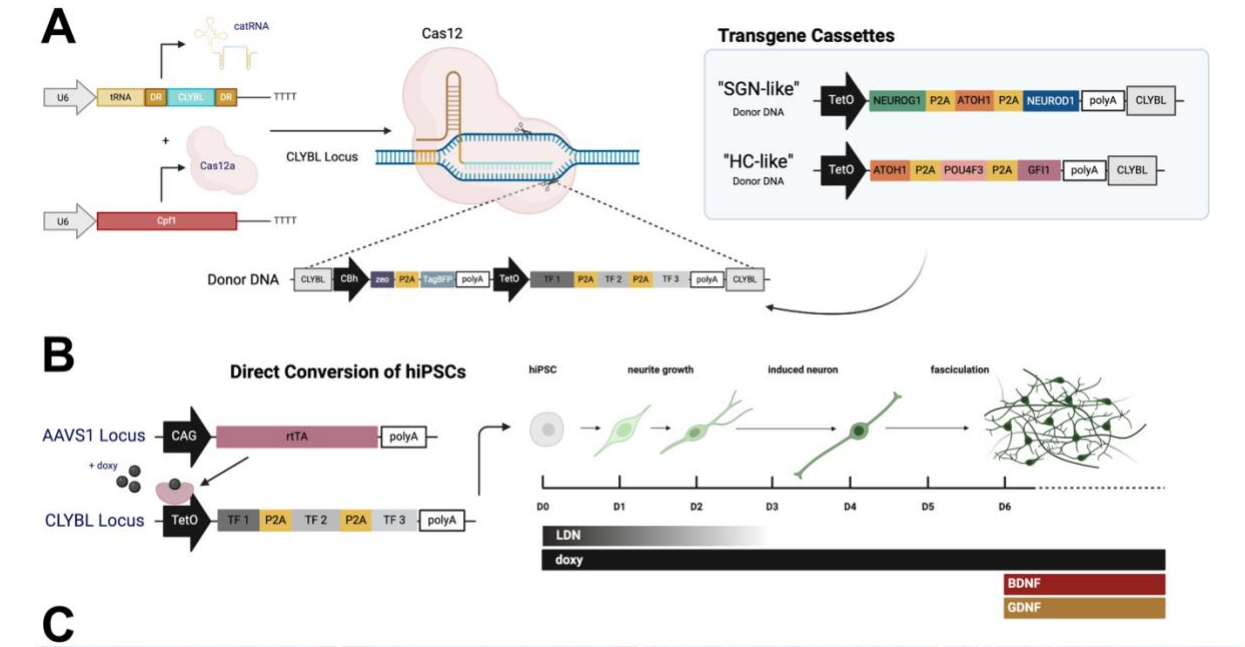
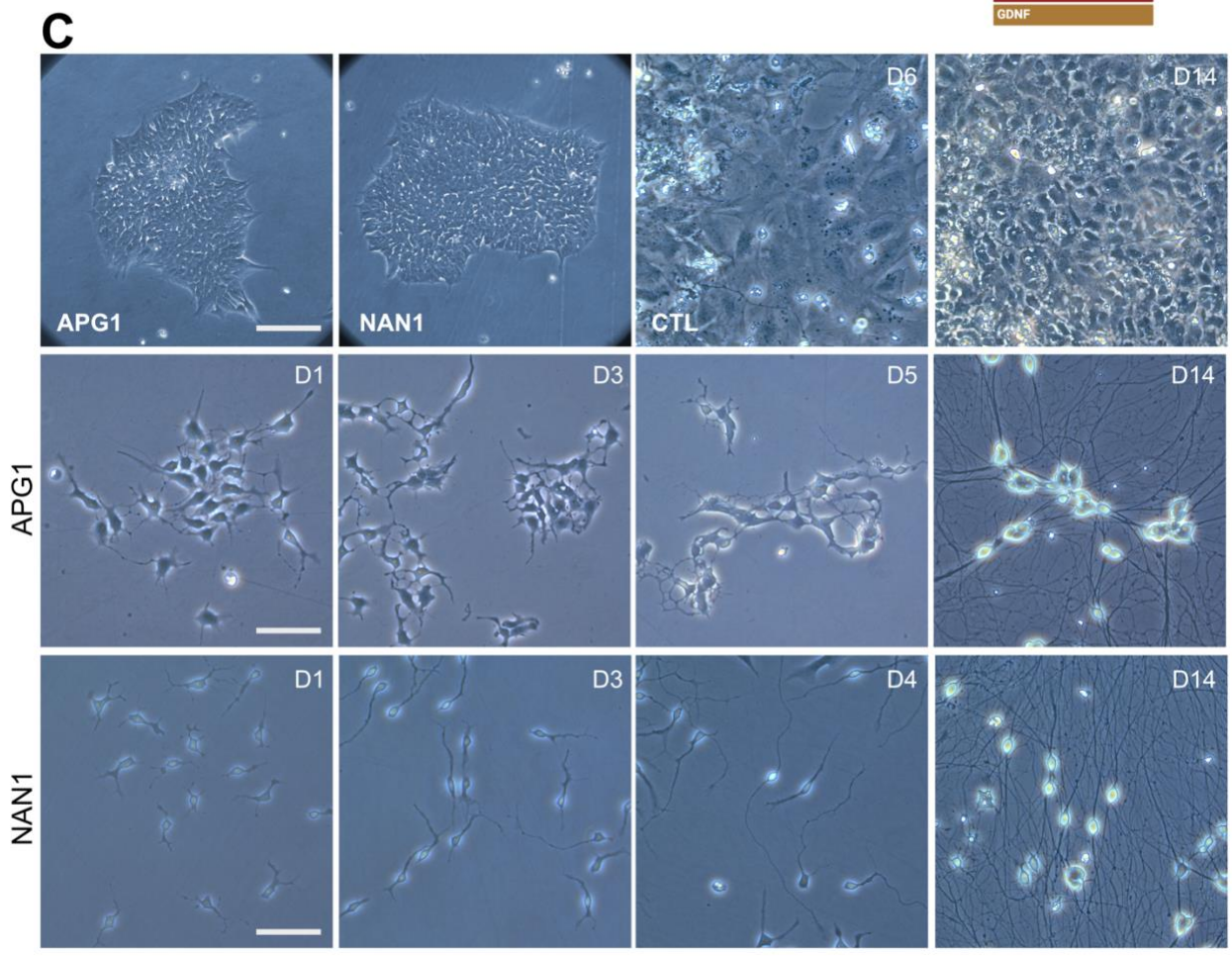

A
Otocyst
D
A
Inner Ear
Cochlea
Saccule
Utricle
Macula Structure in Utricle and Saccule
Otolith
Vestibular ganglion neuron
Vestibular hair cell
OHC
IHC
Organ of Corti
DCs
Type II SGN
PCs
Type I SGN
GER
B
Anterior Domain
Lfng, Sox2, Six1, Eya1
Neurog1
Delaminating neuroblasts
Spiral Ganglion Neuron Development
Gata3
Neurod1
Delta1
Id1
Pou4f1, Rbfox3
Pou4f2
Skil
Cbfb
Pbx1
Thrb, Runx1
Runx1
Id2
Prox1
II
Plk5
Th
Prph
Ia
Calb 2
Pcdh20
Ib
Calb 1/2
Ic
Lypd1, Mgat4c, Pou4f1
Atoh1
Prosensory Cells
Hair Cell Development
p27kip1
Bmp4
FGF2
Hair cell
Pou4f3
Gfi1
Non-sensory supporting cell
Sensory supporting cell
Mature Hair Cell
Tbx2
FGF8
Prox1
FGF3
Inner hair cell
Outer hair cell

Figure 2: Morphological changes of IMR90.4 *APG1* and *NAN1* cell lines upon differentiation. (A-B) High-fidelity CRISPR/Cas12a integrated dox-inducible transgene cassettes [*NEUROG1-p2A-ATOH1-p2A-NEUROD1* (*NAN1*) and *ATOH1-p2A-POU4F3-p2A-GFI1* (*APG1*)] integrated at the CLYBL safe harbor site in IMR90.4 *POU4F3-p2A-eGFP* hiPSC. Diagram of LDN-19318 and dox induction, used for differentiation of hiPSCs. (C) Left two images in first row show undifferentiated *APG1*- and *NAN1*-integrated hiPSCs. Right two images in first row show control cells at days 6 and 14 post-differentiation. Control cells are IMR90.4 *POU4F3-p2A-eGFP* with rtTA-M2 at the AAVS1 site and zeocin resistance marker and empty cassette at CLYBL. They exhibit a flat morphology upon differentiation. Slight neurite outgrowth can be observed at Day 1 for both *NAN1* and *APG1* lines, but cells still appear progenitor-like. The soma and neurites are apparent at Day 3 for *NAN1*, and by Day 7, neurites have grown extensively longer. *APG1* cell bodies appear more elongated and the spindly outgrowths fasciculate at day 5. Scale bar = 100 μm. (A-B) Created with BioRender.com.


A
catRNA
Cas12
U6
tRNA
DR
CLYBL
DR
TTTT
Cas12a
CLYBL Locus
U6
Cpf1
TTTT
Donor DNA
CLYBL
CBh
zeo
P2A
TagBFP
polyA
TetO
TF 1
P2A
TF 2
P2A
TF 3
polyA
CLYBL
Transgene Cassettes
"SGN-like"
Donor DNA
TetO
NEUROG1
P2A
ATOH1
P2A
NEUROD1
polyA
CLYBL
"HC-like"
Donor DNA
TetO
ATOH1
P2A
POU4F3
P2A
GFI1
polyA
CLYBL
B
Direct Conversion of hiPSCs
AAVS1 Locus
CAG
rtTA
polyA
+ doxy
CLYBL Locus
TetO
TF 1
P2A
TF 2
P2A
TF 3
polyA
hiPSC
neurite growth
induced neuron
fasciculation
D0
D1
D2
D3
D4
D5
D6
LDN
doxy
BDNF
GDNF


C
APG1
NAN1
D6
D14
D1
D3
D5
D14
D1
D3
D4
D14

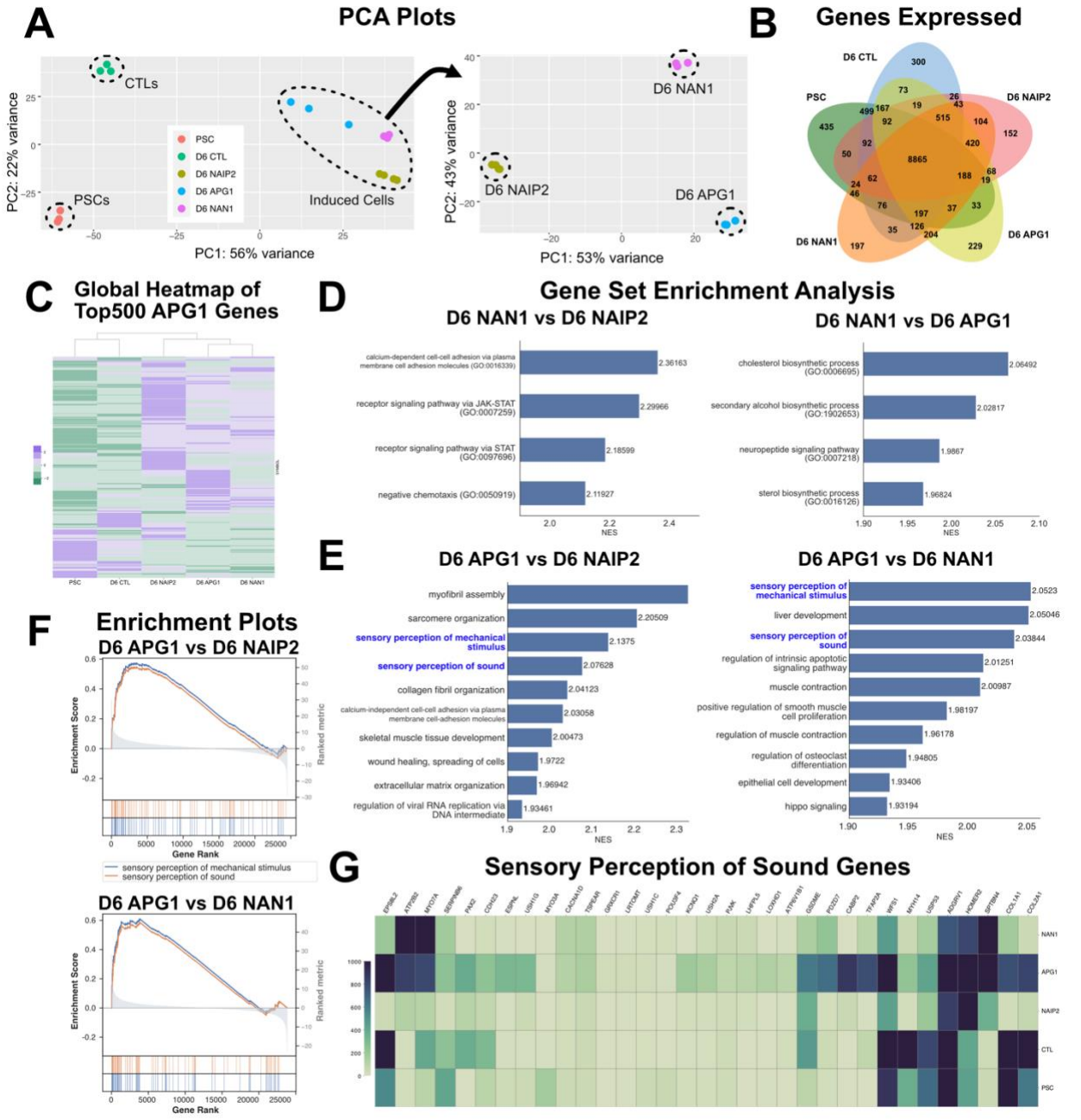


Figure 3: Comparative bulk RNA-seq analyses show *APG1* induced cells heading towards auditory cell fate. (A) Principal component analysis (PCA) plot of hiPSCs, D6 CTL, *NAIP2*, *APG1*, and *NAN1* cells. (B) Venn diagram showing the total and overlapping number of genes expressed in each group (normalized count > 100). (C) Heatmap of the top 500 DEGs in *APG1* cells. (D) Gene enriched pathways in *NAN1* and (E) *APG1* based on ranked list of DEGs. Normalized enrichment scores (NES) are generated based on log2(FC) and FDR<0.05. (F) Genes related to sensory perception of mechanical stimulus and sound are visualized within a ranked list (orange and blue lines) through the enrichment plots. (G) Leading genes in *APG1* for sensory perception of sound pathway are listed in the heat map. Scale represents gene expression counts normalized across rows. FC = fold change; FDR = false discovery rate.

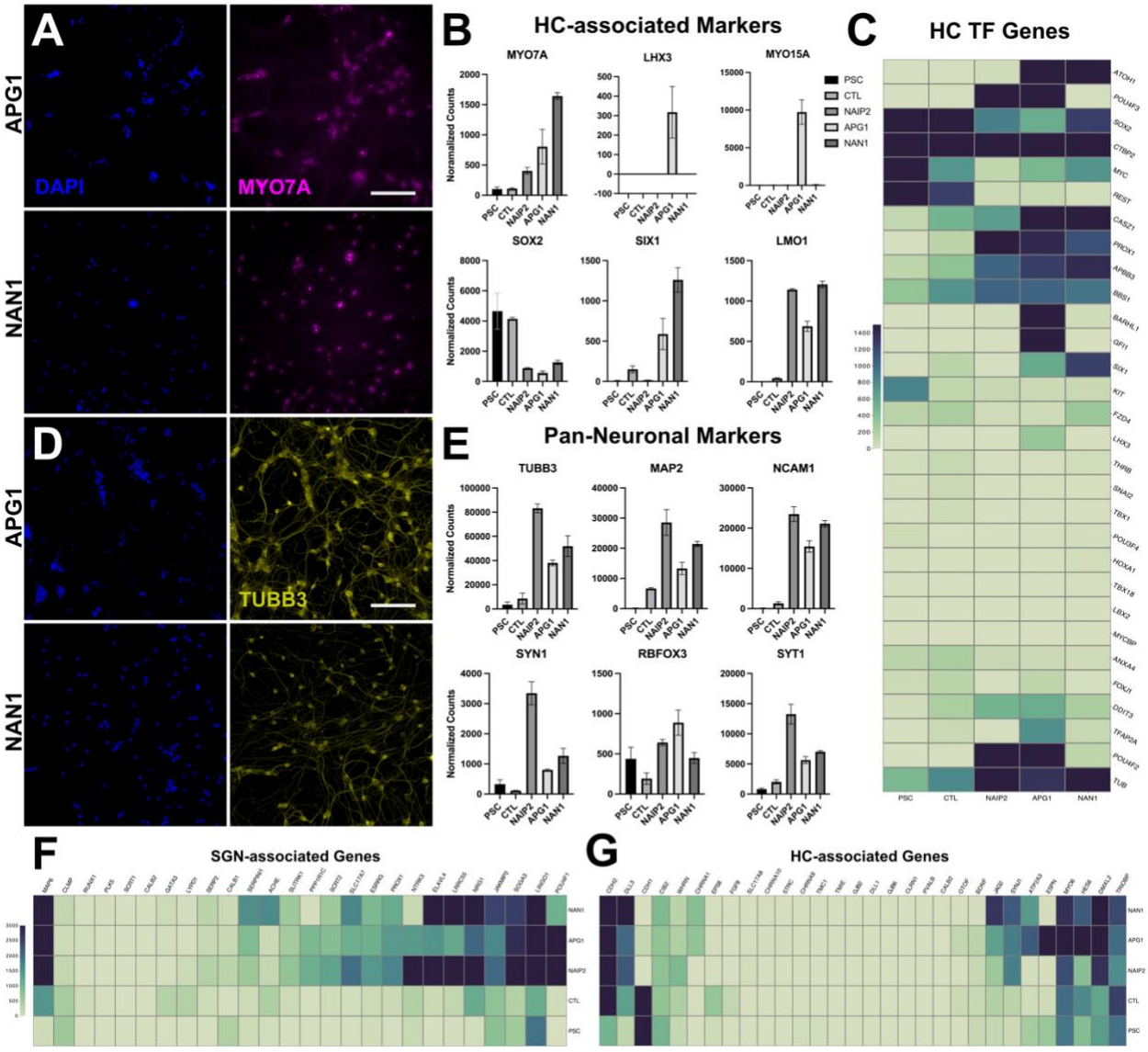
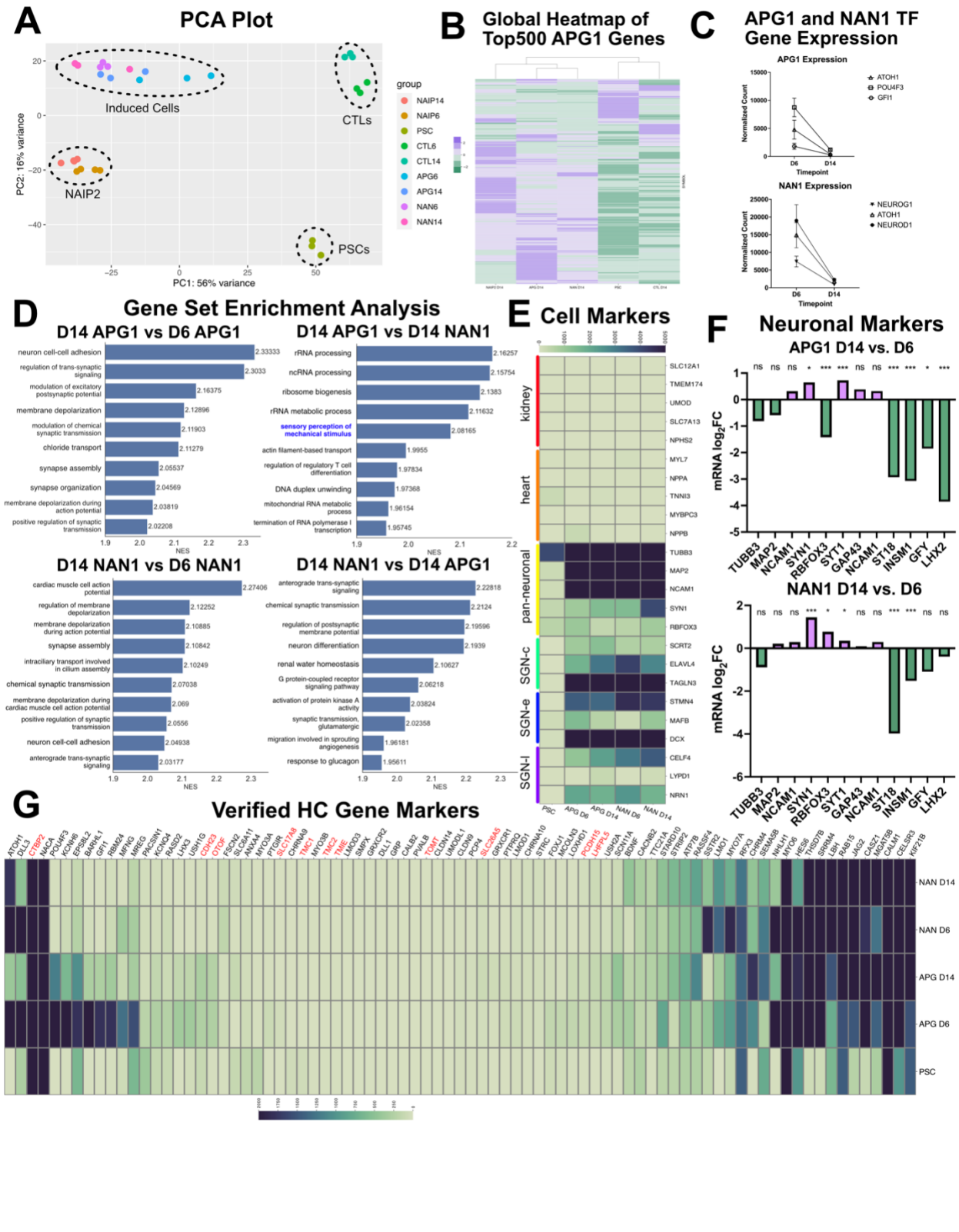


Figure 4: *APG1* and *NAN1* express both HC- and SGN-related genes. (A) Immunostaining of *APG1* and *NAN1* cells at day 6 with DAPI and *MYO7A*. (B) Mean expression of PSC, CTL, *NAIP2*, *APG1*, and *NAN1* at day 6 for HC-associated markers, with error bars showing SEM. (C) Heatmap showing gene expression counts normalized across rows for TF genes involved in HC development. (D) Immunostaining of *APG1* and *NAN1* cells at day 6 with DAPI and *TUBB3*. (E) Mean expression of PSC, CTL, *NAIP2*, *APG1*, and *NAN1* at day 6 for pan-neuronal, with error bars showing SEM. (F-G) Heatmap showing normalized gene expression counts for SGN- and HC-associated genes. Scale bar = 100 μm.

Figure 5: *APG1* and *NAN1* transcriptomic profiles at day 14 overlap with one another. (A) PCA plot of PSCs, CTLs, *NAIP2*, *APG1*, and *NAN1* at days 6 and 14. (B) Global heatmap of the top 500 DEGs in *APG1* at day 14. (C) Line graphs showing normalized expression counts of *ATOH1*, *POU4F3*, and *GFI1* in *APG1* cells at days 6 and 14 and of *NEUROG1*, *ATOH1*, and *NEUROD1* in *NAN1* cells at days 6 and 14. (D) Gene enriched pathways in day 14 *APG1* cells compared to day 6 *APG1* and day 14 *NAN1* (top). Gene enriched pathways in day 14 *NAN1* cells compared to day 6 *NAN1* and day 14 *APG1* (bottom). (E) Heatmap showing normalized expression counts for non-HC-related genes for *APG1* and *NAN1* cells at days 6 and 14. (F) Bar charts showing the $\log_2$ (fold change, FC) between *APG1* at day 14 vs. day 6 (top) and between *NAN1* at day 14 vs. day 6 (bottom) for selected neuronal gene markers. Adjusted p-values were obtained from DGE analysis generated using DESeq2. *P_{adj}<0.05, **P_{adj}<0.01, ***P_{adj}<0.001, ns, not significant. (G) Heatmap showing normalized expression counts for HC-related gene markers. Genes in red represent those involved in the mechanoelectrical transduction channels of HCs.


A
PCA Plot
Induced Cells
CTLs
NAIP2
PSCs
PC1: 56% variance
PC2: 16% variance
B
Global Heatmap of Top500 APG1 Genes
group
NAIP14
NAIP6
PSC
CTL6
CTL14
APG6
APG14
NAN6
NAN14
C
APG1 and NAN1 TF Gene Expression
APG1 Expression
ATOH1
POU4F3
GFI1
Normalized Count
Timepoint
NAN1 Expression
NEUROG1
ATOH1
NEUROD1
D
Gene Set Enrichment Analysis
D14 APG1 vs D6 APG1
neuron cell-cell adhesion
regulation of trans-synaptic signaling
modulation of excitatory postsynaptic potential
membrane depolarization
modulation of chemical synaptic transmission
chloride transport
synapse assembly
synapse organization
membrane depolarization during action potential
positive regulation of synaptic transmission
D14 APG1 vs D14 NAN1
rRNA processing
ncRNA processing
ribosome biogenesis
rRNA metabolic process
sensory perception of mechanical stimulus
actin filament-based transport
regulation of regulatory T cell differentiation
DNA duplex unwinding
mitochondrial RNA metabolic process
termination of RNA polymerase I transcription
D14 NAN1 vs D6 NAN1
cardiac muscle cell action potential
regulation of membrane depolarization
membrane depolarization during action potential
synapse assembly
intraciliary transport involved in cilium assembly
chemical synaptic transmission
membrane depolarization during cardiac muscle cell action potential
positive regulation of synaptic transmission
neuron cell-cell adhesion
anterograde trans-synaptic signaling
D14 NAN1 vs D14 APG1
anterograde trans-synaptic signaling
chemical synaptic transmission
regulation of postsynaptic membrane potential
neuron differentiation
renal water homeostasis
G protein-coupled receptor signaling pathway
activation of protein kinase A activity
synaptic transmission, glutamatergic
migration involved in sprouting angiogenesis
response to glucagon
NES
E
Cell Markers
kidney
heart
pan-neuronal
SGN-c
SGN-e
SGN-l
SLC12A1
TMEM174
UMOD
SLC7A13
NPHS2
MYL7
NPPA
TNNI3
MYBPC3
NPPB
TUBB3
MAP2
NCAM1
SYN1
RBFOX3
SCRT2
ELAVL4
TAGLN3
STMN4
MAFB
DCX
CELF4
LYPD1
NRN1
PSC
APG D6
APG D14
NAN D6
NAN D14
F
Neuronal Markers
APG1 D14 vs. D6
mRNA log2FC
TUBB3
MAP2
NCAM1
SYN1
RBFOX3
SYT1
GAP43
NCAM1
ST18
INSM1
GFY
LHX2
NAN1 D14 vs. D6
G
Verified HC Gene Markers
NAN D14
NAN D6
APG D14
APG D6
PSC

References

1. Haile, L. M., Kamenov, K., Briant, P. S., Orji, A. U., Steinmetz, J. D., Abdoli, A., Abdollahi, M., Abu-Gharbieh, E., Afshin, A., Ahmed, H., Ahmed Rashid, T., Akalu, Y., Alahdab, F., Alanezi, F. M., Alanzi, T. M., Al Hamad, H., Ali, L., Alipour, V., Al-Raddadi, R. M., Amu, H., Arabloo, J., Arab-Zozani, M., Arulappan, J., Ashbaugh, C., Atnafu, D. D., Babar, Z.-U.-D., Baig, A. A., Banik, P. C., Bärnighausen, T. W., Barrow, A., Bender, R. G., Bhagavathula, A. S., Bhardwaj, N., Bhardwaj, P., Bibi, S., Bijani, A., Burkart, K., Cederroth, C. R., Charan, J., Choudhari, S. G., Chu, D.-T., Couto, R. A. S., Dagnew, A. B., Dagnew, B., Dahlawi, S. M. A., Dai, X., Dandona, L., Dandona, R., Desalew, A., Dhamnetiya, D., Dhimal, M. L., Dhimal, M., Doyle, K. E., Duncan, B. B., Ekholuenetale, M., Filip, I., Fischer, F., Franklin, R. C., Gaidhane, A. M., Gaidhane, S., Gallus, S., Ghamari, F., Ghashghaee, A., Ghozali, G., Gilani, S. A., Glavan, I.-R., Golechha, M., Goulart, B. N. G., Gupta, V. B., Gupta, V. K., Hamidi, S., Hammond, B. R., Hay, S. I., Hayat, K., Heidari, G., Hoffman, H. J., Hopf, K. P., Hosseinzadeh, M., Househ, M., Hussain, R., Hwang, B.-F., Iavicoli, I., Ibitoye, S. E., Ilesanmi, O. S., Irvani, S. S. N., Islam, S. M. S., Iwagami, M., Jacob, L., Jayapal, S. K., Jha, R. P., Jonas, J. B., Kalhor, R., Kameran Al-Salihi, N., Kandel, H., Kasa, A. S., Kayode, G. A., Khalilov, R., Khan, E. A., Khatib, M. N., Kosen, S., Koyanagi, A., Kumar, G. A., Landires, I., Lasrado, S., Lim, S. S., Liu, X., Lobo, S. W., Lugo, A., Makki, A., Mendoza, W., Mersha, A. G., Mihretie, K. M., Miller, T. R., Misra, S., Mohamed, T. A., Mohammadi, M., Mohammadian-Hafshejani, A., Mohammed, A., Mokdad, A. H., Moni, M. A., Neupane Kandel, S., Nguyen, H. L. T., Nixon, M. R., Noubiap, J. J., Nuñez-Samudio, V., Oancea, B., Oguoma, V. M., Olagunju, A. T., Olusanya, B. O., Olusanya, J. O., Orru, H., Owolabi, M. O., Padubidri, J. R., Pakshir, K., Pardhan, S., Pashazadeh Kan, F., Pasovic, M., Pawar, S., Pham, H. Q., Pinheiro, M., Pourshams, A., Rabiee, N., Rabiee, M., Radfar, A., Rahim, F., Rahimi-Movaghar, V., Rahman, M. H. U., Rahman, M., Rahmani, A. M., Rana, J., Rao, C. R., Rao, S. J., Rashedi, V., Rawaf, D. L., Rawaf, S., Renzaho, A. M. N., Rezapour, A., Ripon, R. K., Rodrigues, V., Rustagi, N., Saeed, U., Sahebkar, A., Samy, A. M., Santric-Milicevic, M. M., Sathian, B., Satpathy, M., Sawhney, M., Schlee, W., Schmidt, M. I., Seylani, A., Shaikh, M. A., Shannawaz, M., Shiferaw, W. S., Siabani, S., Singal, A., Singh, J. A., Singh, J. K., Singhal, D., Skryabin, V. Y., Skryabina, A. A., Sotoudeh, H., Spurlock, E. E., Taddele, B. W., Tamiru, A. T., Tareque, M. I., Thapar, R., Tovani-Palone, M. R., Tran, B. X., Ullah, S., Valadan Tahbaz, S., Violante, F. S., Vlassov, V., Vo, B., Vongpradith, A., Vu, G. T., Wei, J., Yadollahpour, A., Yahyazadeh Jabbari, S. H., Yeshaw, Y., Yigit, V., Yirdaw, B. W., Yonemoto, N., Yu, C., Yunusa, I., Zamani, M., Zastrozhin, M. S., Zastrozhina, A., Zhang, Z.-J., Zhao, J. T., Murray, C. J. L., Davis, A. C., Vos, T. & Chadha, S. Hearing loss prevalence and years lived with disability, 1990–2019: findings from the Global Burden of Disease Study 2019. *The Lancet* **397**, 996–1009 (2021).

2. Emmett, S. D. & Francis, H. W. The Socioeconomic Impact of Hearing Loss in U.S. Adults. *Otology & Neurotology* **36**, 545–550 (2015).

3. Reed, N. S., Altan, A., Deal, J. A., Yeh, C., Kravetz, A. D., Wallhagen, M. & Lin, F. R. Trends in Health Care Costs and Utilization Associated With Untreated Hearing Loss Over 10 Years. *JAMA Otolaryngol Head Neck Surg* **145**, 27 (2019).

4. Lin, F. R., Metter, E. J., O'Brien, R. J., Resnick, S. M., Zonderman, A. B. & Ferrucci, L. Hearing Loss and Incident Dementia. *Arch Neurol* **68**, (2011).

5. Livingston, G., Huntley, J., Sommerlad, A., Ames, D., Ballard, C., Banerjee, S., Brayne, C., Burns, A., Cohen-Mansfield, J., Cooper, C., Costafreda, S. G., Dias, A., Fox, N., Gitlin, L. N., Howard, R., Kales, H. C., Kivimäki, M., Larson, E. B., Ogunniyi, A., Orgeta, V., Ritchie, K., Rockwood, K., Sampson, E. L., Samus, Q., Schneider, L. S., Selbæk, G., Teri, L. & Mukadam, N. Dementia prevention, intervention, and care: 2020 report of the Lancet Commission. *The Lancet* **396**, 413–446 (2020).

6. Monzani, D., Galeazzi, G. M., Genovese, E., Marrara, A. & Martini, A. Psychological profile and social behaviour of working adults with mild or moderate hearing loss. *Acta Otorhinolaryngol Ital* **28**, 61–66 (2008).

7. Kramer, S. E., Kapteyn, T. S., Kuik, D. J. & Deeg, D. J. H. The Association of Hearing Impairment and Chronic Diseases with Psychosocial Health Status in Older Age. *J Aging Health* **14**, 122–137 (2002).

8. Li, C.-M., Zhang, X., Hoffman, H. J., Cotch, M. F., Themann, C. L. & Wilson, M. R. Hearing Impairment Associated With Depression in US Adults, National Health and Nutrition Examination Survey 2005-2010. *JAMA Otolaryngol Head Neck Surg* **140**, 293 (2014).

9. Kurabi, A., Keithley, E. M., Housley, G. D., Ryan, A. F. & Wong, A. C.-Y. Cellular mechanisms of noise-induced hearing loss. *Hearing Research* **349**, 129–137 (2017).

10. Goutman, J. D., Elgoyhen, A. B. & Gómez-Casati, M. E. Cochlear hair cells: The sound-sensing machines. *FEBS Letters* **589**, 3354–3361 (2015).

11. Wan, G., Corfas, G. & Stone, J. S. Inner ear supporting cells: Rethinking the silent majority. *Seminars in Cell & Developmental Biology* **24**, 448–459 (2013).

12. Wu, D. K. & Kelley, M. W. Molecular Mechanisms of Inner Ear Development. *Cold Spring Harbor Perspectives in Biology* **4**, a008409–a008409 (2012).

13. Morsli, H., Choo, D., Ryan, A., Johnson, R. & Wu, D. K. Development of the Mouse Inner Ear and Origin of Its Sensory Organs. *J. Neurosci.* **18**, 3327–3335 (1998).

14. Kiernan, A. E., Pelling, A. L., Leung, K. K. H., Tang, A. S. P., Bell, D. M., Tease, C., Lovell-Badge, R., Steel, K. P. & Cheah, K. S. E. Sox2 is required for sensory organ development in the mammalian inner ear. *Nature* **434**, 1031–1035 (2005).

15. Zheng, W., Huang, L., Wei, Z.-B., Silvius, D., Tang, B. & Xu, P.-X. The role of Six1 in mammalian auditory system development. *Development* **130**, 3989–4000 (2003).

16. Petitpré, C., Wu, H., Sharma, A., Tokarska, A., Fontanet, P., Wang, Y., Helmbacher, F., Yackle, K., Silberberg, G., Hadjab, S. & Lallemend, F. Neuronal heterogeneity and stereotyped connectivity in the auditory afferent system. *Nat Commun* **9**, 3691 (2018).

17. Shrestha, B. R., Chia, C., Wu, L., Kujawa, S. G., Liberman, M. C. & Goodrich, L. V. Sensory Neuron Diversity in the Inner Ear Is Shaped by Activity. *Cell* **174**, 1229-1246.e17 (2018).

18. Sun, S., Babola, T., Pregernig, G., So, K. S., Nguyen, M., Su, S.-S. M., Palermo, A. T., Bergles, D. E., Burns, J. C. & Müller, U. Hair Cell Mechanotransduction Regulates Spontaneous Activity and Spiral Ganglion Subtype Specification in the Auditory System. *Cell* **174**, 1247-1263.e15 (2018).

19. Kawase, T. & Liberman, M. C. Spatial organization of the auditory nerve according to spontaneous discharge rate. *J of Comparative Neurology* **319**, 312–318 (1992).

20. Anniko, M. Cytodifferentiation of cochlear hair cells. *American Journal of Otolaryngology* **4**, 375–388 (1983).

21. Lanford, P. J., Shailam, R., Norton, C. R., Ridley, T. & Kelley, M. W. Expression of Math1 and HES5 in the Cochleae of Wildtype and Jag2 Mutant Mice. *JARO* **1**, 161–171 (2000).

22. Chessum, L., Matern, M. S., Kelly, M. C., Johnson, S. L., Ogawa, Y., Milon, B., McMurray, M., Driver, E. C., Parker, A., Song, Y., Codner, G., Esapa, C. T., Prescott, J., Trent, G., Wells, S., Dragich, A. K., Frolenkov, G. I., Kelley, M. W., Marcotti, W., Brown, S. D. M., Elkon, R., Bowl, M. R. & Hertzano, R. Helios is a key transcriptional regulator of outer hair cell maturation. *Nature* **563**, 696–700 (2018).

23. Kaiser, M., Lüdtke, T. H., Deuper, L., Rudat, C., Christoffels, V. M., Kispert, A. & Trowe, M.-O. TBX2 specifies and maintains inner hair and supporting cell fate in the Organ of Corti. *Nat Commun* **13**, 7628 (2022).

24. Stone, J. S. & Cotanche, D. A. Hair cell regeneration in the avian auditory epithelium. *Int. J. Dev. Biol.* **51**, 633–647 (2007).

25. Liu, H., Pecka, J. L., Zhang, Q., Soukup, G. A., Beisel, K. W. & He, D. Z. Z. Characterization of Transcriptomes of Cochlear Inner and Outer Hair Cells. *Journal of Neuroscience* **34**, 11085–11095 (2014).

26. Li, Y., Liu, H., Giffen, K. P., Chen, L., Beisel, K. W. & He, D. Z. Z. Transcriptomes of cochlear inner and outer hair cells from adult mice. *Sci Data* **5**, 180199 (2018).

27. Scheffer, D. I., Shen, J., Corey, D. P. & Chen, Z.-Y. Gene Expression by Mouse Inner Ear Hair Cells during Development. *J. Neurosci.* **35**, 6366–6380 (2015).

28. Menendez, L., Trecek, T., Gopalakrishnan, S., Tao, L., Markowitz, A. L., Yu, H. V., Wang, X., Llamas, J., Huang, C., Lee, J., Kalluri, R., Ichida, J. & Segil, N. Generation of inner ear hair cells by direct lineage conversion of primary somatic cells. *eLife* **9**, e55249 (2020).

29. Costa, A., Sanchez-Guardado, L., Juniat, S., Gale, J. E., Daudet, N. & Henrique, D. Generation of sensory hair cells by genetic programming with a combination of transcription factors. *Development* **142**, 1948–1959 (2015).

30. Matern, M. S., Milon, B., Lipford, E. L., McMurray, M., Ogawa, Y., Tkaczuk, A., Song, Y., Elkon, R. & Hertzano, R. GFI1 functions to repress neuronal gene expression in the developing inner ear hair cells. *Development* **147**, dev186015 (2020).

31. Ma, Q., Anderson, D. J. & Fritzsch, B. Neurogenin 1 Null Mutant Ears Develop Fewer, Morphologically Normal Hair Cells in Smaller Sensory Epithelia Devoid of Innervation. *JARO* **1**, 129–143 (2000).

32. Ma, Q., Chen, Z., Barrantes, I. D. B., Luis De La Pompa, J. & Anderson, D. J. neurogenin1 Is Essential for the Determination of Neuronal Precursors for Proximal Cranial Sensory Ganglia. *Neuron* **20**, 469–482 (1998).

33. Petitpré, C., Faure, L., Uhl, P., Fontanet, P., Filova, I., Pavlinkova, G., Adameyko, I., Hadjab, S. & Lallemend, F. Single-cell RNA-sequencing analysis of the developing mouse inner ear identifies molecular logic of auditory neuron diversification. *Nat Commun* **13**, 3878 (2022).

34. Raft, S., Koundakjian, E. J., Quinones, H., Jayasena, C. S., Goodrich, L. V., Johnson, J. E., Segil, N. & Groves, A. K. Cross-regulation of *Ngn1* and *Math1* coordinates the production of neurons and sensory hair cells during inner ear development. *Development* **134**, 4405–4415 (2007).

35. Jahan, I., Pan, N., Kersigo, J. & Fritzsch, B. Beyond generalized hair cells: Molecular cues for hair cell types. *Hearing Research* **297**, 30–41 (2013).

36. Jahan, I., Pan, N., Kersigo, J. & Fritzsch, B. Neurod1 Suppresses Hair Cell Differentiation in Ear Ganglia and Regulates Hair Cell Subtype Development in the Cochlea. *PLoS ONE* **5**, e11661 (2010).

37. Agarwal, D., Dash, N., Mazo, K. W., Chopra, M., Avila, M. P., Patel, A., Wong, R. M., Jia, C., Do, H., Cheng, J., Chiang, C., Jurlina, S. L., Roshan, M., Perry, M. W., Rho, J. M., Broyer, R., Lee, C. D., Weinreb, R. N., Gavrilovici, C., Oesch, N. W., Welsbie, D. S. & Wahlin, K. J. Human retinal ganglion cell neurons generated by synchronous BMP inhibition and transcription factor mediated reprogramming. *npj Regen Med* **8**, 55 (2023).

38. Lyra-Leite, D. M., Fonoudi, H., Gharib, M. & Burridge, P. W. An updated protocol for the cost-effective and weekend-free culture of human induced pluripotent stem cells. *STAR Protocols* **2**, 100213 (2021).

39. Lin, T., Ambasudhan, R., Yuan, X., Li, W., Hilcove, S., Abujarour, R., Lin, X., Hahm, H. S., Hao, E., Hayek, A. & Ding, S. A chemical platform for improved induction of human iPSCs. *Nat Methods* **6**, 805–808 (2009).

40. Wahlin, K. J., Maruotti, J. A., Sripathi, S. R., Ball, J., Angueyra, J. M., Kim, C., Grebe, R., Li, W., Jones, B. W. & Zack, D. J. Photoreceptor Outer Segment-like Structures in Long-Term 3D Retinas from Human Pluripotent Stem Cells. *Sci Rep* **7**, 766 (2017).

41. Gossen, M., Freundlieb, S., Bender, G., Müller, G., Hillen, W. & Bujard, H. Transcriptional Activation by Tetracyclines in Mammalian Cells. *Science* **268**, 1766–1769 (1995).

42. Brewer, G. J., Torricelli, J. R., Evege, E. K. & Price, P. J. Optimized survival of hippocampal neurons in B27-supplemented neurobasal^{TM}, a new serum-free medium combination. *J of Neuroscience Research* **35**, 567–576 (1993).

43. Bardy, C., Van Den Hurk, M., Eames, T., Marchand, C., Hernandez, R. V., Kellogg, M., Gorris, M., Galet, B., Palomares, V., Brown, J., Bang, A. G., Mertens, J., Böhnke, L., Boyer, L., Simon, S. & Gage, F. H. Neuronal medium that supports basic synaptic functions and activity of human neurons in vitro. *Proc. Natl. Acad. Sci. U.S.A.* **112**, (2015).

44. Cerbini, T., Funahashi, R., Luo, Y., Liu, C., Park, K., Rao, M., Malik, N. & Zou, J. Transcription Activator-Like Effector Nuclease (TALEN)-Mediated CLYBL Targeting Enables Enhanced Transgene Expression and One-Step Generation of Dual Reporter Human Induced Pluripotent Stem Cell (iPSC) and Neural Stem Cell (NSC) Lines. *PLOS ONE* **10**, e0116032 (2015).

45. Pujades, C., Kamaid, A., Alsina, B. & Giraldez, F. BMP-signaling regulates the generation of hair-cells. *Developmental Biology* **292**, 55–67 (2006).

46. Kitano, T., Kitajiri, S.-I., Nishio, S.-Y. & Usami, S.-I. Detailed Clinical Features of Deafness Caused by a Claudin-14 Variant. *Int J Mol Sci* **20**, 4579 (2019).

47. Ben-Yosef, T. Claudin 14 knockout mice, a model for autosomal recessive deafness DFNB29, are deaf due to cochlear hair cell degeneration. *Human Molecular Genetics* **12**, 2049–2061 (2003).

48. Gong, J., Qian, P., Hu, Y., Guo, C., Wei, G., Wang, C., Cai, C., Wang, H. & Liu, D. Claudin h Is Essential for Hair Cell Morphogenesis and Auditory Function in Zebrafish. *Front. Cell Dev. Biol.* **9**, 663995 (2021).

49. Cai, T., Jen, H.-I., Kang, H., Klisch, T. J., Zoghbi, H. Y. & Groves, A. K. Characterization of the transcriptome of nascent hair cells and identification of direct targets of the Atoh1 transcription factor. *J Neurosci* **35**, 5870–5883 (2015).

50. Sato, M. P., Benkafadar, N. & Heller, S. Hair cell regeneration, reinnervation, and restoration of hearing thresholds in the avian hearing organ. *Cell Reports* **43**, 113822 (2024).

51. Klisch, T. J., Xi, Y., Flora, A., Wang, L., Li, W. & Zoghbi, H. Y. In vivo *Atoh1* targetome reveals how a proneural transcription factor regulates cerebellar development. *Proc. Natl. Acad. Sci. U.S.A.* **108**, 3288–3293 (2011).

52. Li, C., Li, X., Bi, Z., Sugino, K., Wang, G., Zhu, T. & Liu, Z. Comprehensive transcriptome analysis of cochlear spiral ganglion neurons at multiple ages. *eLife* **9**, e50491 (2020).

53. Oyer, J. A., Chu, A., Brar, S. & Turker, M. S. Aberrant Epigenetic Silencing Is Triggered by a Transient Reduction in Gene Expression. *PLoS ONE* **4**, e4832 (2009).

54. Kues, W. A., Schwinzer, R., Wirth, D., Verhoeyen, E., Lemme, E., Herrmann, D., Barg-Kues, B., Hauser, H., Wonigeit, K., Niemann, H., Kues, W. A., Schwinzer, R., Wirth, D., Verhoeyen, E., Lemme, E., Herrmann, D., Barg-Kues, B., Hauser, H., Wonigeit, K. & Niemann, H. Epigenetic silencing and tissue independent expression of a novel tetracycline inducible system in double-transgenic pigs. *FASEB j.* **20**, 1200–1202 (2006).

55. Pankiewicz, R., Karlen, Y., Imhof, M. O. & Mermod, N. Reversal of the silencing of tetracycline-controlled genes requires the coordinate action of distinctly acting transcription factors. *The Journal of Gene Medicine* **7**, 117–132 (2005).

56. Wu, C.-C., Brugeaud, A., Seist, R., Lin, H.-C., Yeh, W.-H., Petrillo, M., Coppola, G., Edge, A. S. B. & Stankovic, K. M. Altered expression of genes regulating inflammation and synaptogenesis during regrowth of afferent neurons to cochlear hair cells. *PLoS ONE* **15**, e0238578 (2020).

57. Qiu, X. & Müller, U. Mechanically Gated Ion Channels in Mammalian Hair Cells. *Front. Cell. Neurosci.* **12**, 100 (2018).

58. Driver, E. C., Sillers, L., Coate, T. M., Rose, M. F. & Kelley, M. W. The Atoh1-lineage gives rise to hair cells and supporting cells within the mammalian cochlea. *Developmental Biology* **376**, 86–98 (2013).

59. Erni, S. T., Gill, J. C., Palaferri, C., Fernandes, G., Buri, M., Lazarides, K., Grandgirard, D., Edge, A. S. B., Leib, S. L. & Roccio, M. Hair Cell Generation in Cochlear Culture Models Mediated by Novel γ-Secretase Inhibitors. *Front. Cell Dev. Biol.* **9**, 710159 (2021).

60. Kelley, M. W., Xu, X.-M., Wagner, M. A., Warchol, M. E. & Corwin, J. T. The developing organ of Corti contains retinoic acid and forms supernumerary hair cells in response to exogenous retinoic acid in culture. *Development* **119**, 1041–1053 (1993).

61. Represa, J., Sanchez, A., Miner, C., Lewis, J. & Giraldez, F. Retinoic acid modulation of the early development of the inner ear is associated with the control of *c-fos* expression. *Development* **110**, 1081–1090 (1990).

62. Zhong, C., Chen, Z., Luo, X., Wang, C., Jiang, H., Shao, J., Guan, M., Huang, L., Huang, X. & Wang, J. Barhl 1 is required for the differentiation of inner ear hair cell-like cells from mouse embryonic stem cells. *The International Journal of Biochemistry & Cell Biology* **96**, 79–89 (2018).

63. Hume, C. R., Bratt, D. L. & Oesterle, E. C. Expression of LHX3 and SOX2 during mouse inner ear development. *Gene Expression Patterns* **7**, 798–807 (2007).